Chemical Engineering Journal 417 (2021) 129302

Contents lists available at ScienceDirect

Chemical Engineering Journal

journal homepage: www.elsevier.com/locate/cej

Synergistic effect of functionalized ionic liquid and alkanolamines mixed solution on enhancing the mass transfer of CO_2 absorption in microchannel

Daofan Ma, Chunying Zhu *, Taotao Fu, Youguang Ma *, Xigang Yuan

State Key Laboratory of Chemical Engineering, School of Chemical Engineering and Technology, Tianjin University, Tianjin 300072, China

ARTICLE INFO

Keywords:
CO_2 capture
Ionic liquid
Alkanolamines
Microchannel
Mass transfer

ABSTRACT

A novel hybrid absorbent by combining functionalized ionic liquid (IL) 1-(3-aminopropyl)-3-methylimidazolium tetrafluoroborate [Apmim][BF_4] with alkanolamines (monoethanolamine (MEA) and N, N-diethylethanolamine (DEEA)) was proposed for CO_2 capture. By means of a high-speed camera, the capacity and mass transfer performance of CO_2 absorption into the hybrid absorbent were investigated experimentally in microchannel over a wide range of concentration ratios (IL: amine) at the room temperature and atmosphere pressure. Three flow patterns were observed: Taylor-bubbly flow, Taylor flow and Taylor-annular flow. The results show that the CO_2 loading and mass transfer coefficient of alkanolamine solution could be improved remarkably by the addition of an appropriate amount of [Apmim][BF_4]. The molar ratio 3:2 of IL to amine was found to be optimal for CO_2 loading and mass transfer. Furthermore, the influences of gas and liquid flow rates on mass transfer were studied, and a new predicting correlation for CO_2 volumetric mass transfer coefficient was proposed.

1. Introduction

The excessive emission of CO_2 in the atmosphere has become a challenging issue of global concern, which leads to catastrophic climate warming and greenhouse effect. Highly efficient CO_2 capture technique is the most effective method to solve the problem [1]. Currently, amine-based CO_2 capture and store is a widely used method through the recycling of absorbent [2]. The common alkanolamines include primary amines, secondary amines, tertiary amines, hindered amines and their mixed amine solutions. However, alkanolamines usually have some inherent deficiencies such as corrosiveness, larger solvent consumption and the regeneration energy consumption, thus, novel solvents with high efficiency, easy regeneration and small consumption are strongly needed, which have motivated increasing interest of researchers [3,4].

Ionic liquids (ILs), a kind of salts composed solely of anions and cations, have been proved to have many advantages for CO_2 absorption over the traditional solvents, such as low volatility, high thermal and chemical stability. Furthermore, ILs are recognized as the green solvent environmentally-friendly, which shows considerably promising perspectives in electrochemistry, catalysis, extraction, cellulose processing and analytical chemistry [5–7]. The solubility of CO_2 in ILs could be adjusted by altering the ion pair interaction of cation and anion, this is especially conducive to the energy-saving gas separation and further solvent regeneration [8]. The physical and chemical properties of ILs rely primarily on the cations and anions. The CO_2 absorption into conventional ionic liquids is controlled mainly by physical absorption mechanism, which usually leads to the lower CO_2 capacity and the less solubility range of only 0.10% to 0.15% (mass fraction) [9]. To be more effective, some functionalized ILs were designed and synthesized, particularly, the ILs functionalized by amine and amino acid groups show excellent CO_2 capture and regeneration performance [10–12]. Generally, the functionalized ILs are also called as task-specific ionic liquids. Zareiekordshouli et al. [13] investigated the absorption performance of CO_2 into functionalized ionic liquids [Amim][Tf_2N], it was found that the capture performance of [Amim][Tf_2N] at low pressure ($\leq$1bar) is similar to that of chemical solvents. Moreover, both the absorption capacity and rate are much more than conventional ILs solution due to the presence of an attached primary amine group to the imidazolium cation.

Nevertheless, ILs have also the drawback of high viscosity, in particular, functionalized IL has relatively high viscosity. In addition, the high cost and operating expense of ILs also limit their industrial applications for the absorption and desorption processes. Consequently, the development of more efficient and cost-effective solvent is imperatively required. The combination of IL with alkanolamines could reduce the regeneration energy consumption, improve the physical properties (viscosity, corrosiveness, volatility and so on) of solvents and increase

* Corresponding authors.
E-mail addresses: zhchy971@tju.edu.cn (C. Zhu), ygma@tju.edu.cn (Y. Ma).

https://doi.org/10.1016/j.cej.2021.129302
Received 24 December 2020; Received in revised form 3 March 2021; Accepted 5 March 2021
Available online 12 March 2021

Nomenclature

a	specific surface area, m^{-1}
A	surface area, m^2
B	base B
C	concentration, $mol \cdot m^{-3}$
C^*	equilibrium concentration of CO_2 in the liquid phase, $mol \cdot m^{-3}$
Ca	Capillary number, dimensionless ($Ca = \mu u/\sigma$)
d_h	hydraulic diameter, m
D	diffusion coefficient, $m^2 \cdot s^{-1}$
E	enhancement factor
E_i	instantaneous enhancement factor
f	bubble formation frequency, Hz
f_{cir}	circulation frequency in liquid slug, Hz
h	specific parameters, $m^3 \cdot mol^{-1}$
H	Henry constant, $mol \cdot m^{-3} \cdot Pa^{-1}$
Ha	Hatta number
k_L	liquid-side overall mass transfer coefficient, $m \cdot s^{-1}$
k_La	liquid-side overall volumetric mass transfer coefficient, s^{-1}
k_{ov}	overall reaction rate constant, s^{-1}
$k_{2,i}$	second-order reaction rate constant in i solution (i = MEA, DEEA, IL), $m^3 \cdot mol^{-1} \cdot s^{-1}$
k_p	liquid-side physical mass transfer coefficient, $m \cdot s^{-1}$
l	length, m
m	number of bubbles generated in time t
N	mass transfer flux, $mol \cdot m^{-2} \cdot s^{-1}$
P	pressure, Pa
Q	flow rate, $m^3 \cdot s^{-1}$
R	gas constant, $J \cdot mol^{-1} \cdot K^{-1}$
Re	Reynolds number, dimensionless ($Re = \rho u d_h/\mu$)
Sc	Schmidt number, dimensionless ($Sc = \mu_L/D\rho_L$)
Sh	Sherwood number, dimensionless ($Sh = k_L d_h/D$)
T	temperature, K
U	velocity, $m \cdot s^{-1}$
V	volume, m^3
r	corner radius, m
t	time, s
w_c	microchannel width, m

Greek letters

α	CO_2 loading, $mol \cdot kg^{-1}$
ρ	density, $kg \cdot m^{-3}$
μ	viscosity, Pa·s
σ	surface tension, $N \cdot m^{-1}$

Subscripts

b	bubble
G	gas-phase
ion	ion
In	microchannel inlet
L	liquid
Out	microchannel outlet
s	slug
tp	gas–liquid two-phase

the absorption capacity of CO_2 [14,15]. IL-amine mixtures have been developed for CO_2 capture, such as [Bmim][BF_4]-MEA [1,16,17], [Emim][Tf_2N]-MEA[18], [N_{1111}] [Gly]-MDEA [19]. Based on CFD simulation, Pishnamazi et al. [17] compared the CO_2 removal efficiency by MEA and MEA + [Bmim][BF_4] solution in membrane contactors. The results indicated that the addition of 30% [Bmim][BF_4] to MEA could significantly improve the CO_2 mass transfer performance, the removal efficiency was increased from 18% to 79%. Feng et al. [19] synthesized a functionalized ionic liquids [N_{1111}][Gly], which was mixed with MDEA for CO_2 absorption, the solubility and absorption rate of CO_2 in IL-MDEA hybrid solvent were investigated. Results showed that the addition of [N_{1111}][Gly] could significantly improve the absorption rate of CO_2 in MDEA aqueous solution. The aqueous solution of 15 wt% IL + 15 wt% MDEA indicated the highest absorption rate and absorption capacity than other mixed solution with same total concentration of 30 wt%, the regeneration efficiency exceeded 98%.

Compared to [Bmim][BF_4], the interactions of chemical bonds between the amine-based functionalized ionic liquid [Apmim][BF_4] and CO_2 molecules greatly increase the absorption capacity because of an extra amino group on cation [20–22], Meanwhile, the viscosity of [Apmim][BF_4] could be distinctly reduced in aqueous solutions, this is very important for absorption process. Moreover, the low volatility of solvent avoids the secondary pollution to the environment. Recently, the novel tertiary amine DEEA received special attention due to its good selectivity, large absorption capacity, high alkalinity and easy synthesis from cheap sustainable renewable raw material. It has been reported that DEEA has higher reaction rate than MDEA owing to its higher basicity [23]. However, the reaction rate of DEEA has with CO_2 is lower. Therefore, the primary/secondary amines (such as MEA) were added into DEEA to increase the CO_2 absorption rate [24,25]. Jiang et al. [26] studied the reaction kinetics of CO_2 absorption into MEA-DEEA aqueous solutions, they perceived that the reaction rate of MEA-DEEA solution with CO_2 was higher than DEEA alone. To overcome the high energy consumption and strong corrosiveness of alkanolamines, in this study, the alkanolamines (MEA-DEEA) is combined with functionalized ionic liquid [Apmim][BF_4] as a novel hybrid absorbent for CO_2 absorption to attain higher mass transfer performance and lower regeneration energy consumption.

Microreactor could achieve more effective mass and heat transfer due to its higher specific surface area and shorter diffusion length, generally, the mass transfer coefficient may be increased by 1 to 3 orders of magnitude in comparison with conventional reactor [27,28]. Moreover, microreactor has many merits including safety, controllability, small sample requirement and flexibility, and so forth, consequently, it has been widely used in a variety of fields such as chemical engineering, pharmacy, medicine, energy [29,30]. Aghel et al. [31] studied CO_2 absorption into three solvents of MEA, DEA, and a-MDEA in microchannel reactor under different operating conditions. The results showed a remarkable enhancement in mass transfer for all three solvents in comparison with other absorption devices. Akkarawatkhoosith et al. [32] investigated the application of microchannel contactor for CO_2 capture (water as absorbent), particularly for CO_2-rich gas. They found the microchannel technology could increase the CO_2 absorption efficiency for the CO_2-rich gas and the maximum absorption efficiency could achieve 70.9%.

At present, although many studies have been conducted on CO_2 absorption into ionic liquids, less focused on the mechanism of CO_2 absorption by functionalized ionic liquids. Especially, the CO_2 absorption mechanism by ILs-amine mixed solution as absorbent in the microreactor remains still far from fully understanding. In this study, a new hybrid solvent [Apmim][BF_4]-MEA-DEEA aqueous solution was proposed for CO_2 capture. The capacity and mass transfer of CO_2 absorption into IL-amine solutions were investigated systematically in microreactor. Based on the two-film theory and solute penetration theory, the influences of gas and liquid flow rates on mass transfer were studied. Meanwhile, the CO_2 loading and mass transfer coefficient were investigated at different IL-amine molar ratios. Furthermore, the CO_2 absorption mechanism in the IL-amine mixed solution was analyzed.

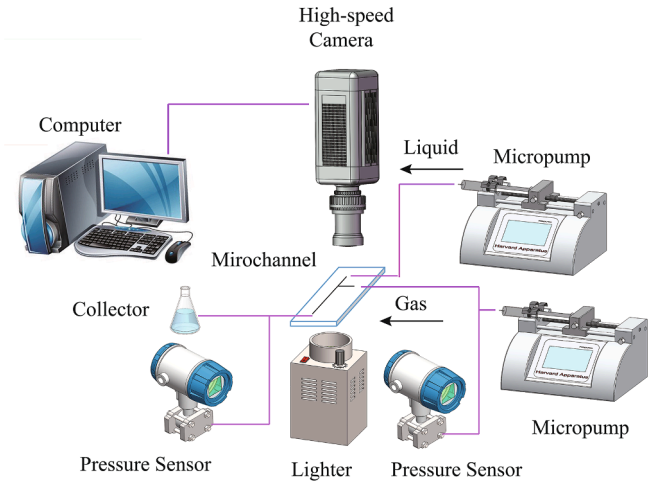

Fig. 1. Schematic diagram of the experimental setup.

2. Experiment

2.1. Experimental setup and materials

The microchannel device used in the present work is a T-shaped microchannel, made of Polymethylmethacrylate (PMMA). The channel has 400 μm depth with a square cross-section. The main channel length is 30 mm, and the length of gas and liquid phase inlet are both 8 mm. The experimental setup is shown in Fig. 1, including syringe pump (Harvard Apparatus, PHD2000, USA), high-speed camera (Motion Pro Y-5, USA), microchannel chip, cold light source, pressure sensor (Honeywell ST3000, USA), collector, and computer.

The dry CO_2 (mass purity ≥ 99%, Tianjin Jinganda Co., Ltd.) was employed as the gas phase. The 1-(3-aminopropyl)-3-methyl-imidazolium tetrafluoroborate ([Apmim][BF_4]) (mass purity ≥ 95%, Shanghai Chengjie Chemical Reagent Co. Ltd.) + monoethanolamine (MEA) (mass purity ≥ 99%, Aladdin Chemical Reagent Co. Ltd.) + 2-(Diethylamino) ethanol (DEEA) (mass purity ≥ 99%, Aladdin Chemical Reagent Co. Ltd.) blended solution was used as the liquid phase. The surfactant, sodium dodecyl sulfate (SDS) was added into liquid phase at a fixed mass fraction of 0.3% to maintain the stability of two-phase system. The molecule structure of chemicals is depicted in Fig. 2.

Total concentrations of IL and amines in the liquid phase were fixed in 1 mol·L^{-1}, namely $C_{IL} + C_{amine} = 1$ mol·L^{-1}, here $C_{amine} = C_{MEA} + C_{DEEA}$. According to previous study [33], at a given concentration of MEA-DEEA solution, the molar ratio 1:4 of MEA to DEEA has the best desorption performance and higher regeneration rate. Therefore, the molar ratio of MEA to DEEA in this work is fixed to 1:4. The density (ρ), viscosity (μ) and surface tension (σ) of the liquid phase were measured by a densitometer (Anton Paar, Austria), an iVisc capillary viscometer (iVisc, LAUDA, Germany) and a surface tension meter (OCAH200, Data Physics instruments GmbH, Germany), respectively. The physical properties of IL-amine aqueous solutions are summarized in Table 1.

2.2. Experimental procedure

The dispersed phase CO_2 gas and the continuous phase IL-amine solutions were fed into the microchannels through two syringe pumps, respectively. The IL-amine solutions were injected from the main channel, and the CO_2 was fed from the branch channel. The bubbles were generated at the T-junction and absorbed by the liquid phase along the channel. The experiments were carried out under room temperature and atmospheric pressure (T = 298.15 K, P = 101.325 kPa), and the pressure drop was measured by the pressure sensors in real time. The liquid flow rate was set from 20 mL·h^{-1} to 80 mL·h^{-1}, and the gas flow rate was controlled in the range of 10–650 mL·h^{-1}. A high-speed camera and image processing software were used for recording the movement of bubbles and liquid slugs along the microchannel. The camera was set at 3008 × 80 pixels resolution and 1000 fps frame frequency.

3. Theoretical analysis

3.1. Calculation method

As the pure CO_2 was used in the experiment, thus the mass transfer resistance of gas phase is negligible, according to the two-film theory, the mass transfer flux of CO_2 could be calculated by:

$$N_{CO_2} = \frac{dn_{CO_2}}{Adt} = k_L(C^* - C) \quad (1)$$

where N_{CO_2} is the mass transfer flux of CO_2, n_{CO_2} is the mole amount of CO_2, A is the total surface area of the bubble, t is the time, k_L is the liquid-side overall mass transfer coefficient, C^* is the equilibrium concentration of CO_2, and C is the concentration of CO_2 in liquid.

Based on the ideal-gas equation:

$$N_{CO_2} = \frac{dn_{CO_2}}{Adt} = m\frac{d(PV_b)}{ARTdt} = \frac{f(P_{in}V_{in} - P_{out}V_{out})}{ART} \quad (2)$$

where m is the number of bubbles generated in time t, P and V_b is the pressure and the volume of a single bubble, R is the ideal gas constant, T is the temperature, f is the bubble generation frequency. P_{in} and V_{in} are the gas pressure and bubble volume at the inlet, respectively; P_{out} and V_{out} are gas pressure and bubble volumes at the outlet of the

Table 1
The physical properties of Liquid phase.

[Apmim][BF_4]/ (mol·L^{-1})	Amine/ (mol·L^{-1})	ρ/(g·cm^{-3})	μ/(mPa·s)	σ/(mN·m^{-1})
0	1	0.99483	1.475	40.13
0.1	0.9	1.00411	1.398	37.64
0.2	0.8	1.00657	1.361	36.88
0.3	0.7	1.01181	1.337	36.01
0.4	0.6	1.01602	1.330	35.89
0.5	0.5	1.02180	1.326	34.73
0.6	0.4	1.02856	1.321	34.05
0.7	0.3	1.03353	1.306	33.26
0.8	0.2	1.04046	1.254	33.11

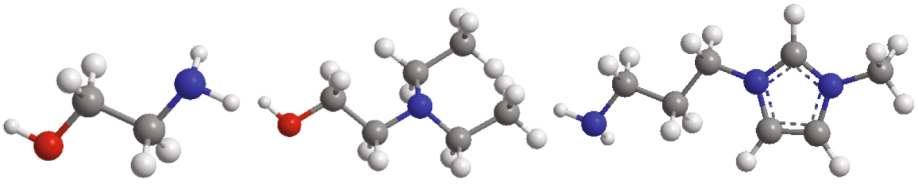

(a) (b) (c)

Fig. 2. Molecular structure (red: O atom; blue: N atom; gray: C atom; white: H atom). (a) MEA, (b) DEEA, (c) Structure of cation in [Apmim][BF_4] (For interpretation of the references to colour in this figure legend, the reader is referred to the web version of this article.)

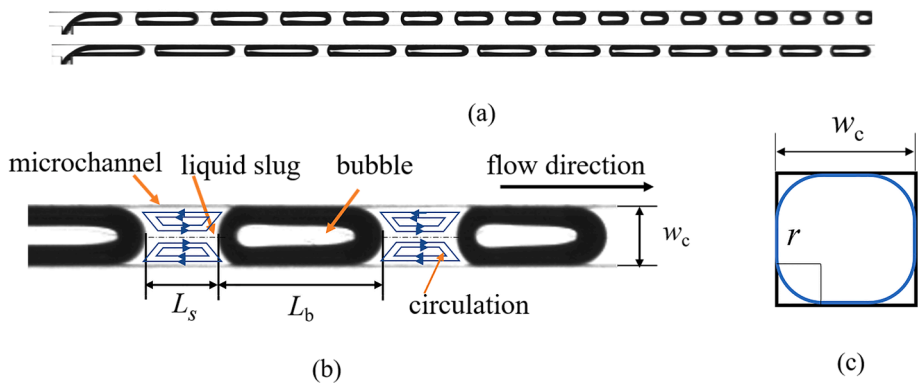

Fig. 3. Schematic of gas–liquid two-phase flow in the microchannel: (a) typical captured images, (b) bubble shape, (c) bubble cross-section.

microchannel, respectively.

As the concentrations of alkanolamines and ionic liquid in the liquid phase remain nearly constant during the absorption process, thus the reaction between CO_2 and IL-amine could be considered as pseudo first-order reaction [20,34]. Besides, because the CO_2 absorption is a rapid reaction [20,26], and the liquid phase is excessive, thus the concentration of CO_2 in the liquid phase could be regarded as zero. Combining Eq. (1) and (2), k_L could be obtained:

$$k_L = \frac{f(P_{in}V_{in} - P_{out}V_{out})}{ARTC^*} \tag{3}$$

The equilibrium concentration C^* can be obtained from Henry coefficient:

$$C^* = H_{CO_2}P_{CO_2} \tag{4}$$

where H_{CO_2} represents the Henry's constant of CO_2 in the mixed solution and P_{CO_2} denotes the average pressure in the microchannel. Because the [Apmim][BF_4] aqueous solution is ionic, the Schumpe model could be used to estimate the Henry's constant of CO_2 in IL-amine aqueous solution[35,36]:

$$log(H_{CO_2,w}/H_{CO_2}) = \sum(h_{ion} + h_G)C_{ion} \tag{5}$$

$$h_G = h_{G,0} + h_T(T - 298.15) \tag{6}$$

$$H_{CO_2,w} = 3.54 \times 10^{-7} exp(2044/T) \tag{7}$$

where $H_{CO_2,w}$ is the Henry's constant of CO_2 in water, h_{ion} and h_G are the ion and gas specific parameters. C_{ion} is the molar concentration of the ion, h_T reflects the effect of temperature on the gas specific parameters, $h_{G,0}$ is constant and equal to -0.0172 $m^3 \cdot kmol^{-1}$. The value of h_{ion} for some ions or CO_2 could be obtained from the literature [35]. When the value of h_{ion} for an ion is unknown, it could be estimated by a similar species, such as the h_{ion} of the cation $[Apmim]^+$ could be estimated by $h_{NH_4^+}$, $h_{HCO_3^-}$ could be estimated by $h_{CO_3^{2-}}$ [37]. The $h_{[BF4]^-}$ was calculated according to the literature [38]. Consequently, based on Eqs. (4)-(7), the Henry's constant of CO_2 in IL-amine solution could be obtained.

The CO_2 loading (α) is defined as:

$$\alpha = \frac{\text{accumulated absorption capacity (mol } CO_2)}{\text{mass of absorbent (kg)}} \tag{8}$$

In the study, Taylor flow regime was primarily investigated as shown in Fig. 3 (a), and the bubble capillary numbers Ca_b were always less than 0.04. In this case, the bubble and liquid slug could be appropriately simplified for calculating the volume V_b and surface area A_b of a single bubble: (1) the length of the bubbles and liquid slugs are uniform; (2) the bubble caps are regarded as hemispheres, while the cross-section of bubble main body is not circular as shown in Fig. 3 (c). Then the volume and surface area of a bubble could be calculated by Eqs. (9) and (10) [39]:

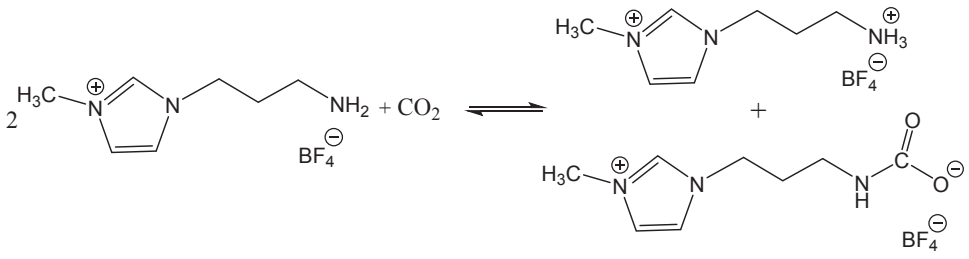

$$V_b = \pi w_c^3/6 + (0.95w_c)^2(l_b - w_c) \tag{9}$$

$$A_b = \pi w_c^2 + [2\pi r + 4(w_c - 2r)](l_b - w_c) \tag{10}$$

where w_c is the microchannel width, l_b is the bubble length, and r is the corner radius.

3.2. Reaction mechanism

The quaternary ammonium salt and carbamate were generated in one step via the reaction between CO_2 and [Apmim][BF_4], indicating that the reaction stoichiometric ratio of [Apmim][BF_4] to CO_2 is 2:1.

(11)

The chemical reaction of CO_2 absorption into MEA solution accords with the zwitterionic reaction mechanism. Firstly, MEA reacts with CO_2 to form a zwitterion, then, the zwitterion combines with a base B to form carbamate and protonated base BH^+. The main bases could be DEEA, [Apmim][BF_4] or H_2O. However, according to the base-catalyzed hydration mechanism [26], the reaction of tertiary amine DEEA solution

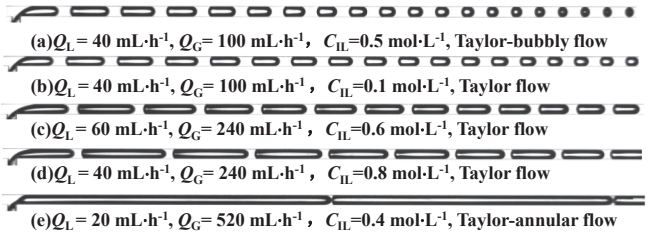

Fig. 4. Gas-liquid two-phase flow pattern in the microchannel.

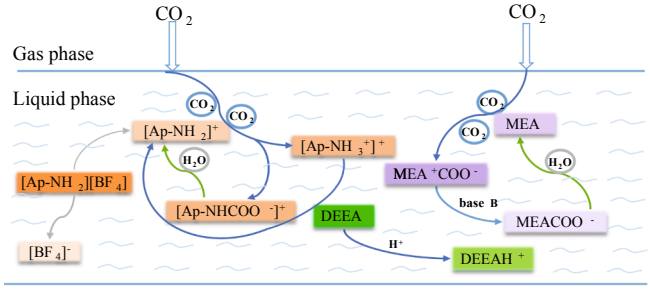

Fig. 6. Reaction mechanism of CO_2 with [Apmim][BF_4]-MEA-DEEA.

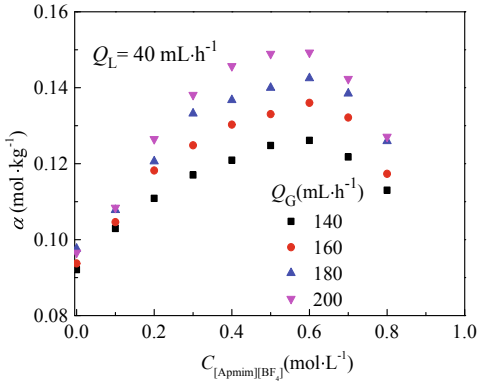

Fig. 5. CO_2 loading in different molar ratios of IL-amine aqueous solutions.

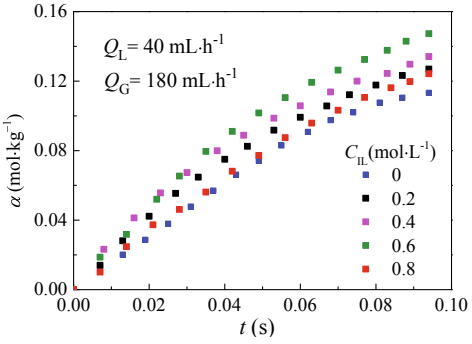

Fig. 7. CO_2 loading of IL-amine solutions versus time.

absorption CO_2 would form bicarbonate, as DEEA can't react directly with CO_2, instead, it acts only as an alkaline substance to catalyze the hydration reaction between CO_2 and OH^-.

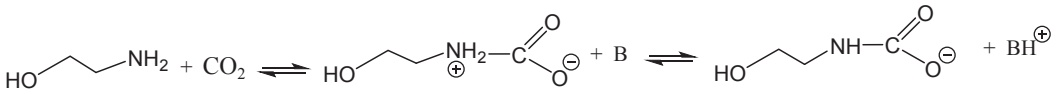

(12)

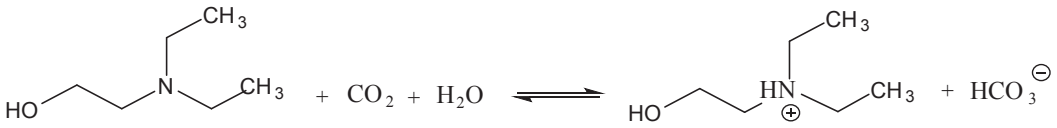

(13)

4. Result and discussion

4.1. Flow regime

Three flow patterns were observed under the experimental conditions: (I) Taylor-bubbly flow, (II) Taylor flow and (III) Taylor-annular flow, as shown in Fig. 4. (I) When the liquid flow rate is maintained at constant and the gas flow rate is relatively lower, the short Taylor-shaped bubbles were generated at the T-junction. The Taylor bubbles would evolve gradually into spherical gas bubbles due to the chemical absorption and disperse uniformly in the liquid phase and flow along the channel. (II) Subsequently, the flow regime would evolve into the Taylor flow with the increase of gas-phase superficial velocity, its apparent characteristic is the alternating appearance between bubbles and liquid slugs. Moreover, the bubbles are wrapped by a thin liquid film and separated by a liquid slug, their lateral size is approximate to the channel width. When the gas phase flow rate is further risen, the bubble length and the bubble formation frequency increase until the Taylor-annular flow appears. (III) Under the Taylor-annular flow, the Taylor bubbles are almost joined together, there is not visible liquid slugs between bubbles. The shape and number of bubbles depend mainly on the gas and liquid phase flow rates.

The gas–liquid two-phase flow pattern relies primarily on following factors: (1) fluid physical properties, such as viscosity, density, compressibility, etc.; (2) microchannel material properties, such as surface tension, wall wettability; (3) microchannel structure; (4) the gas and liquid phase superficial flow velocity. Sun et al. [40] observed the gas–liquid two phase flow patterns using N_2 and H_2O as dispersed and continuous phases in rectangular microchannels with different cross-sections. They also found similar flow regimes with our experiments and studied the influence of microchannel configuration on the flow regime distribution and the transition law between different flow patterns. Generally, the Taylor flow regime is the most widely used flow pattern as it could offer a relatively steady flow state, wide operating

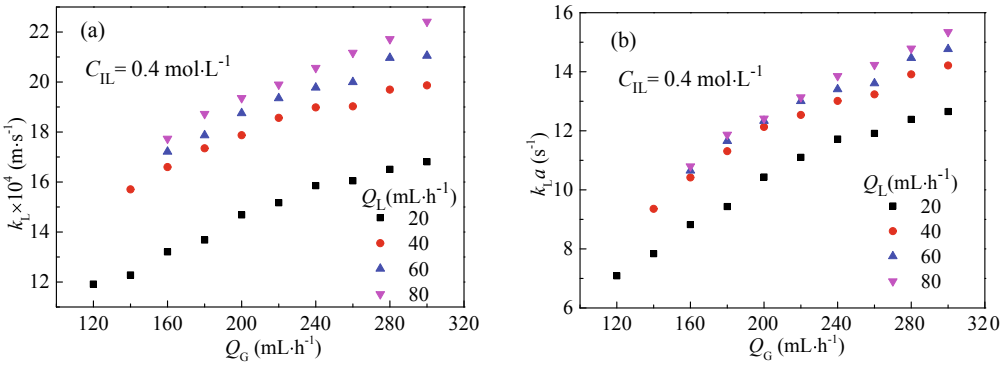

Fig. 8. The effect of gas and liquid flow rates on mass transfer (C_{IL} = 0.4 mol·L^{-1}). (a) liquid-side mass transfer coefficient, (b) liquid-side overall volumetric mass transfer coefficient.

range and low axial dispersion, which is conducive to the mass transfer between gas and liquid two phases. Therefore, this study would also be focused on the absorption and mass transfer characteristics under Taylor flow.

4.2. CO_2 loading in the IL-amine aqueous solution

The CO_2 loading of IL-amine aqueous solution with different molar ratios of IL to amine is shown in Fig. 5. It could be found that an appropriate addition of [Apmim][BF_4] could effectively promote the CO_2 absorption in comparison with MEA-DEEA solution. With the increase of ionic liquid concentration, the CO_2 loading firstly increases and then gradually decreases, this is similar to other functionalized ionic liquid-amine mixed aqueous solutions [19]. Meanwhile, it could be seen from Fig. 5 that the aqueous solutions of 0.6 mol·L^{-1} IL and 0.4 mol·L^{-1} alkanolamines indicates the higher CO_2 loading than other IL-amine solutions with 1 mol·L^{-1} total concentration.

Fig. 6 illustrates the chemical reaction mechanism between [Apmim][BF_4]-DEEA-MEA and CO_2. As the [Apmim][BF_4] ([Ap-NH_2][BF_4]) concentration rises, a part of [Apmim][BF_4] acted as a base to participate in the deprotonation of the MEA zwitterion to form carbamate ($MEACOO^-$), and the another reacts with CO_2 to generate the IL carbamate [Ap-$NHCOO^-$]$^+$. Since the carbamate ($MEACOO^-$ and [Ap-$NHCOO^-$]$^+$) has an intrinsic H proton, which could combine with H_2O molecule to form hydrate and thereby cause the intramolecular hydrolysis to regenerate MEA and [Apmim][BF_4]. Additionally, DEEA as a proton acceptor could interact with the protonated quaternary ammonium salt ([Ap-NH_3^+]$^+$) to regenerate the [Apmim][BF_4] [41]. Meanwhile, it could also interact with MEA zwitterion to yield carbamate ($MEACOO^-$), which could hydrolyze to regenerate MEA. Consequently, the total reaction rate could be enhanced due to the synergistic effect of functionalized ionic liquid and alkanolamines, leading to higher CO_2 loading.

From Fig. 5, the CO_2 loading increases with ion liquid concentration and reaches the maximum at C_{IL} = 0.6 mol·L^{-1}. As IL concentration is further increased, which would lead to a decrease in C_{amine} concentration, consequently, the CO_2 loading starts to decline. This is due to that the promotion effect of ionic liquid on alkanolamines becomes weakened, a similar phenomenon was also observed in the literature [22]. In addition, as shown in Table 1, the increase of [Apmim][BF_4] concentration would cause the decrease of viscosity of IL-amine solution, this is beneficial for the CO_2 absorption. Comparatively, the contribution of synergistic effect on the CO_2 loading is dominant over that of viscosity decrease. The optimum ratio of IL to amine is 3:2 under constant liquid total concentration of 1 mol·L^{-1}.

The variation of CO_2 loading in aqueous solutions of [Apmim][BF_4]-MEA-DEEA with time is illustrated in Fig. 7, it could be clearly seen from Fig. 7 that the CO_2 loading at C_{IL} = 0.6 mol·L^{-1} was larger than that at other IL concentrations within the same absorption time. As IL concentrations are 0.2, 0.4, 0.6 and 0.8 mol·L^{-1}, respectively, compared to the situation without addition of IL, the CO_2 loading is improved as 12.10%, 18.46%, 30.12% and 5.78% correspondingly. Moreover, it could also be observed from Fig. 7 that the CO_2 loading increases rapidly at first due to the positive contribution of the chemical reaction and then its increment gradually slows down. According to Eq. (11), the absorption efficiency of [Apmim][BF_4] for CO_2 relies strongly on the functionalized chain (primary amine group) appended to the IL cation [13]. In the starting stage, Alkanolamine or IL could quickly absorb CO_2 to produce zwitterion or carbamate, subsequently, the effectively reactive components decrease, and thereby the increase of CO_2 loading becomes slowed down. In industrial application, the IL-based mixture with higher CO_2 capacity could reduce the requirement of liquid circulation amount, accordingly cutting down the energy consumption of liquid pump [21].

Table 2
The frequency of circulations under different operating conditions at C_{IL} = 0.4 mol·L^{-1}.

Q_L (mL·h^{-1})	Q_G (mL·h^{-1})	f_{cir} (Hz)
40	140	169.232
40	160	201.248
40	180	240.659
40	200	282.651
20	160	151.061
60	160	206.219
80	160	208.980

4.3. Mass transfer performance of CO_2 into IL-amine aqueous solutions

4.3.1. Effects of gas and liquid flow rates on mass transfer

The mass transfer between gas and liquid two phases is primarily stemming from two parts: (1) the mass transfer between the bubble body and surrounding liquid film, which depends mainly on the contact time; (2) the mass transfer between bubble caps and the liquid slug, which relies primarily on the circulation. For the mass transfer process accompanied by rapid chemical reaction, the gas side mass transfer resistance could be neglected as the gas diffusion coefficient is relatively large, especially when pure CO_2 gas is utilized, the mass transfer resistance depends completely on the liquid side.

Fig. 8(a) indicates the evolution of the liquid-side mass transfer coefficient k_L with the gas and liquid flow rates. The results show that the increase of gas or liquid flow rate could improve k_L. This is because the increase of fluid flow rate could reduce the thickness of the interfacial diffusion layer and decrease the mass transfer resistance, hence the mass transfer is enhanced, and k_L increases. Besides, the bubble residence time would become shortened once the gas or liquid phase superficial flow velocity rises. According to the solute permeation theory, the shorter gas–liquid contact time would lead to steeper concentration

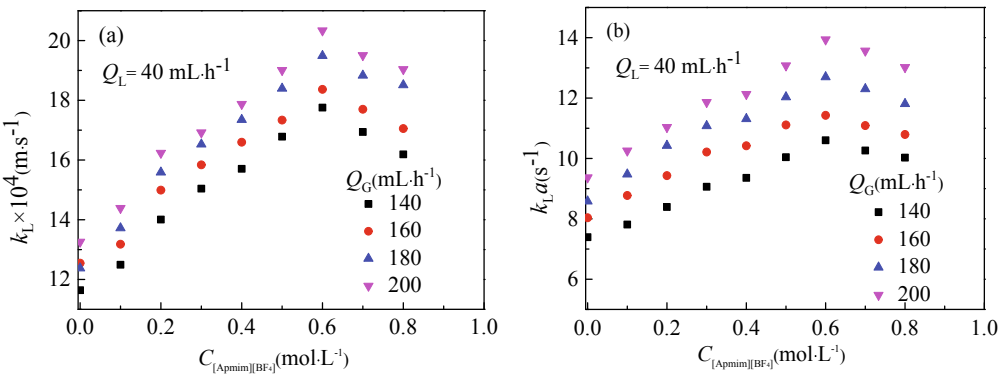

Fig. 9. The effect of [Apmim][BF_4] concentration on mass transfer. (a) liquid-side overall mass transfer coefficient, (b) liquid-side overall volumetric mass transfer coefficient.

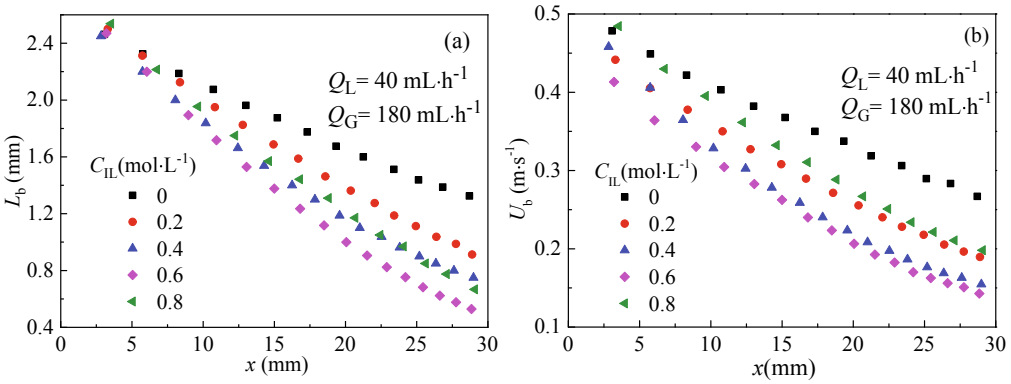

Fig. 10. Hydraulic properties under different [Apmim][BF_4] concentration. (a) bubble length, (b) bubble velocity.

distribution curve, which facilitates CO_2 diffusion at the interface and enhances the gas–liquid mass transfer [42].

In addition, the occurrence of internal circulation in the liquid slug could also greatly intensify mass transfer [43]. Due to the obstruction action of bubble, the liquid near the slug center has to flow towards back, which promotes the radial mass transfer of CO_2. The vortex intensity increases with increasing gas or liquid flow rate, thus the mass transfer intensification also becomes remarkable correspondingly. The internal circulation in liquid slug was first found by Thulasidas et al. [44] using particle imaging velocimetry (PIV). Theoretically, the formation of circulation is resulting from the velocity difference between the bubble and the liquid slug. The frequency of circulations f_{cir} reflects the amount of mass transfer per unit of time [43]:

$$f_{cir} = \frac{U_{tp} - U_b/2}{2L_s} \tag{14}$$

where U_{tp} is gas–liquid two-phase superficial flow velocity, U_b is the bubble velocity, and L_s is the liquid slug length. The f_{cir} in the liquid slug adjacent to the stable bubble under various operating conditions are listed in Table 2. It could be found that the circulation frequency increase with gas or liquid flow rate, higher gas velocity would form shorter liquid slug and more internal circulation, consequently, the mass exchange between the liquid film and the liquid slug, and the gas–liquid surface renewal are greatly enhanced, as a result, the significant gas–liquid mass transfer intensification is attained.

It could be seen from Fig. 8(b) that the liquid-side overall volumetric mass transfer coefficient k_La increases with the gas or liquid flow rate in which a is the specific surface area defined as the ratio of total bubble surface area to the microchannel volume. At a given liquid flow rate, the increase of gas flow rate would lead to the increase of the bubble length and the decrease of liquid slug length, thus the effective area for gas–liquid mass transfer is increased. Conversely, when the gas flow rate is fixed, the bubble length becomes shortened with increasing the liquid phase flow rate, thus the specific surface area reduces. Therefore, for a constant Q_L, the increase of k_La with Q_G could be primarily attributed to the increase of a. In contrast, for a constant Q_G, the increase of k_La with Q_L should be owing to the increase of k_L (Fig. 8a).

4.3.2. *Effect of [Apmim][BF_4] concentration on mass transfer*

Fig. 9 shows the effect of [Apmim][BF_4] concentration on mass transfer. It indicates that the increase of [Apmim][BF_4] concentration could improve mass transfer. The variation of k_L with C_{IL} could be divided into two stages: (I) C_{IL} less than 0.6 mol·L^{-1}, in this stage, the increase of IL concentration could result in apparent rise of the liquid side mass transfer coefficient; (II) C_{IL} greater than 0.6 mol·L^{-1}, in this stage, k_L decreases with C_{IL}.

When the gas and liquid flow rates are constant, the effect of IL concentration on the mass transfer coefficient depends mainly on three factors. Firstly, the chemical reaction between the liquid phase and CO_2 would directly affect the bubble length L_b and the bubble velocity U_b, accordingly influence the internal circulation in the liquid slug and the mass exchange between the liquid film and the liquid slug. Secondly, the CO_2 diffusion is closely related to the viscosity of liquid phase, lower viscosity is conducive to the CO_2 absorption. Moreover, for gas–liquid mass transfer companied with chemical reaction, the mass transfer coefficient also hinges on the reaction rate [11]. Thus, k_L is actually a competitive result between above three factors.

In the first stage, the IL-amine synergistic effect is enhanced due to the increase of [Apmim][BF_4] concentration, which promotes CO_2 absorption and accordingly leads to the shortening of the bubble as shown in Fig. 10(a), where × represents the distance from the bubble to the T-junction. Meanwhile, the reaction rate between CO_2 and IL + amine is

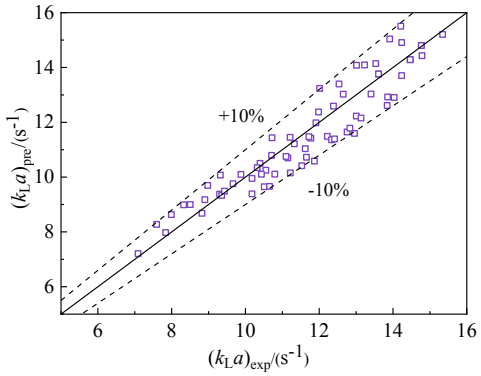

Fig. 11. Comparison between experimental data and predicting values of k_La.

enlarged, which could cause the shift of reaction location toward gas–liquid interface and the reduction of the mass transfer resistance on the liquid side [45], therefore, mass transfer was enhanced. However, the bubble velocity becomes slowed down (Fig. 10(b)), consequently, the internal circulation in the liquid slug and the mass exchange between liquid film and liquid slug become weakened, this is not conducive to k_L. The jointly competitive effect of above factors leads to the increase of k_L at this stage, in which the most important contribution is chemical reaction. In the second stage, the further increase of IL concentration indicates negative influence on the mass transfer (Fig. 7). The rise of bubble velocity (Fig. 10) could result in the intensification of internal circulation in the liquid slug with increasing IL concentration, correspondingly, the mass transfer is enhanced. Besides, the IL-amine mixed aqueous solution with higher IL concentration has lower viscosity (Table 1), which is in favor of the molecule diffusion and mass transfer. However, the reaction rate decreases at higher ion liquid concentration, therefore, leading to the decline of mass transfer coefficient. Comparatively, the effect of the chemical reaction on mass transfer is more important than the liquid physical property and internal circulation in liquid slug. The variation trend of k_La with IL concentration is similar to k_L.

4.4. Prediction of mass transfer coefficient

According to various experiments, some different correlations for physical absorption processes have been proposed to predict mass transfer coefficients in microchannel [46,47]:

$$Sh_L \cdot a \cdot d_h = 0.084 Re_G^{0.213} \cdot Re_L^{0.937} \cdot Sc_L^{0.5} \tag{15}$$

$$Sh_L \cdot a \cdot d_h = 0.094 Re_G^{0.0656} \cdot Re_L^{0.654} \cdot Sc_L^{1.449} \cdot Ca_{tp}^{0.839} \tag{16}$$

where *Sh* represents the ratio of convective mass transfer to diffusion mass transfer, *Sc* is the ratio of kinematic viscosity coefficient to diffusion coefficient, *Re* reflects the flow conditions, and *Ca* is the ratio of fluid viscosity to interfacial tension.

However, the all previous proposed correlations in the literatures are unsuitable for the absorption with chemical reaction due to the significant influence of chemical reaction on mass transfer. Therefore, the enhancement factor of chemical reaction on mass transfer was considered to modify the physical absorption model.

$$Sh_L \cdot a \cdot d_h = \beta_1 Re_G^{\beta_2} Re_L^{\beta_3} Sc_L^{0.5} Ca_L^{\beta_4} E^{\beta_5} \tag{17}$$

where $Sh_L = k_L\, d_h/D$, $Re_G = \rho_G\, u_G\, d_h/\mu_G$, $Re_L = \rho_L\, u_L\, d_L/\mu_L$, $Ca_L = \mu_L\, u_L/\sigma$, $Sc_L = \mu_L/D\rho_L$, ρ, σ, μ are density, surface tension and viscosity, respectively. d_h is the equivalent diameter of the microchannel, and D is the diffusion coefficient of CO_2 in the liquid phase (estimated by literature [48]). The enhancement factor E reflects the enhancement of chemical reaction on mass transfer, which could be obtained from the model proposed by Van Krevelen and Hoftijzer [49]:

$$E = \frac{Ha\sqrt{(E_i - E)/(E_i - 1)}}{tanhHa\sqrt{(E_i - E)/(E_i - 1)}} \tag{18}$$

where Ha is the Hatta number, E_i is the instantaneous enhancement factor based on the solute penetration theory:

$$Ha = \sqrt{D_{CO_2} k_{ov}} \Big/ k_p \tag{19}$$

$$E_i = 1 + \frac{C_{amine} D_{amine}}{C^* D_{CO_2}} \tag{20}$$

where k_{ov} represents the overall reaction rate constant and could be presented as $k_{ov} = k_{2,MEA} C_{MEA} + k_{2,DEEA} C_{DEEA} + k_{2,IL} C_{IL}$ (the second-order rate coefficient $k_{2,MEA}$, $k_{2,DEEA}$, $k_{2,IL}$ were taken from the literatures [20,26]). k_p is the liquid-side physical mass transfer coefficient.

The diffusivity of amine into the mixed solution D_{amine} could be calculated using the method given in the literature [50]. By fitting experimental data, the parameters in Eq. (17) could be obtained: $\beta_1 = 0.168$, $\beta_2 = 0.495$, $\beta_3 = 1.101$, $\beta_4 = 1.033$, $\beta_5 = 0.421$. The comparison between calculated values by Eq. (17) and experimental data was shown in Fig. 11, and the relative deviation is less ± 10%, which indicates good prediction performance.

5. Conclusion

The mixed aqueous solution of functionalized ionic liquid ([Apmim][BF_4]) and alkanolamines (MEA: DEEA = 1:4) was proposed as a novel absorbent for CO_2 capture. The absorption capacity and mass transfer performance of CO_2 into the novel absorbent were investigated experimentally. Three flow patterns were observed: Taylor-bubbly flow, Taylor flow, and Taylor-annular flow. The mass transfer could be remarkably enhanced with the rise of gas and liquid flow rates due to the increased internal circulation frequency in liquid slug. The optimum concentration ratio of IL to amine was 3:2, at this ratio, the new hybrid absorbent showed higher CO_2 loading and larger mass transfer coefficient under total solution concentration of 1 mol·L^{-1}. When the concentration ratio was less than 3:2, the synergistic effect of absorbent enhanced with increasing [Apmim][BF_4] concentration, which promoted chemical absorption and hence intensified mass transfer. When the concentration ratio was larger than 3:2, the synergistic effect of IL and amine became weakened, accordingly the CO_2 loading and mass transfer coefficient reduced. The synergistic effect of hybrid absorbent on gas–liquid mass transfer for CO_2 absorption was found to be the most significant at IL = 0.6 mol·L^{-1}. A new correlation was proposed for predicting the liquid-side overall volumetric mass transfer coefficient of chemical absorption process, the calculated result confirms the good accuracy of the present correlation.

Declaration of Competing Interest

The authors declare that they have no known competing financial interests or personal relationships that could have appeared to influence the work reported in this paper.

Acknowledgments

This work was supported by the National Natural Science Foundation of China (Nos. 21776200, 21978197).

References

[1] M. Xiao, H. Liu, H. Gao, W. Olson, Z. Liang, CO_2 capture with hybrid absorbents of low viscosity imidazolium-based ionic liquids and amine, Appl. Energ. 235 (2019) 311–319.

[2] H. Ling, S. Liu, T. Wang, H. Gao, Z. Liang, Characterization and correlations of CO_2 absorption performance into aqueous amine blended solution of monoethanolamine (MEA) and N, N-Dimethylethanolamine (DMEA) in a packed column, Energ. Fuel 33 (2019) 7614–7625.

[3] L.C. Barbosa, O.d.Q.F. Araújo, J.L.d. Medeiros, Ionic liquid [Bmim][NTf_2] as solvent for CO_2 removal in offshore processing of natural gas, Mater. Sci. Forum 965 (2019) 21–28.

[4] Y.L. Wang, Y.G. Liu, X.B. Liu, G.X. Li, J.G. Qi, J.W. Yang, Z.Y. Zhu, Y.X. Ma, J. Gao, F.Q. Meng, Novel postcombustion capture process for CO_2 from the flue gas of coal-fired power plants using a green deep eutectic solvent, ACS Sustain. Chem. Eng. 8 (2020) 2236–2245.

[5] Z. Zhang, Y. Liu, Y. Dai, H. Zhang, Z. Chen, Y. Shen, Z. Zhu, Y. Wang, Life cycle environmental implications of ionic-liquid-based carbon capture and storage processes and its alternative improvement cases, ACS Sustain. Chem. Eng. 8 (2020) 18106–18113.

[6] C. Chen, Y. Ma, D. Zheng, L. Wang, J. Li, J. Zhang, H. He, S. Zhang, Insight into the role of weak interaction played in the fixation of CO_2 catalyzed by the amino-functionalized imidazolium-based ionic liquids, J. CO2. Util. 18 (2017) 156–163.

[7] R. Chokkareddy, N. Thondavada, N.K. Bhajanthri, G.G. Redhi, An amino functionalized magnetite nanoparticle and ionic liquid based electrochemical sensor for the detection of acetaminophen, Anal. Methods 11 (2019) 6204–6212.

[8] M. Aghaie, N. Rezaei, S. Zendehboudi, A systematic review on CO_2 capture with ionic liquids: Current status and future prospects, Renew. Sust. Energ. Rev. 96 (2018) 502–525.

[9] X. Zhou, G. Jing, F. Liu, B. Lv, Z. Zhou, Mechanism and kinetics of CO_2 absorption into an aqueous solution of a triamino-functionalized ionic liquid, Energ Fuel 31 (2017) 1793–1802.

[10] B. Lv, J. Wu, C. Lin, Z. Zhou, G. Jing, Kinetic and heat duty study of aprotic heterocyclic anion-based dual functionalized ionic liquid solutions for carbon capture, Fuel 263 (2020), 116676.

[11] Y. Meng, X. Wang, F. Zhang, Z. Zhang, Y. Wu, IL-DMEE Nonwater System for CO_2 Capture: Absorption Performance and Mechanism Investigations, Energ. Fuel 32 (2018) 8587–8593.

[12] B. Lv, G. Jing, Y. Qian, Z. Zhou, An efficient absorbent of amine-based amino acid-functionalized ionic liquids for CO_2 capture: High capacity and regeneration ability, Chem. Eng. J. 289 (2016) 212–218.

[13] F. Zareiekordshouli, A. Lashani-zadehgan, P. Darvishi, Thermophysical properties and CO_2 absorption studies of the amine functionalized [Amim][Tf_2N] and the non-functionalized counterpart [bmim][Tf_2N] ionic liquids, Int. J. Greenh. Gas. Con 53 (2016) 328–337.

[14] F. Zhang, L. Guo, Y. Ding, X. Zhu, Q. Liao, Flow pattern and CO_2 absorption in a falling film reactor with mixed aqueous solution of ionic liquid and MEA, Appl. Therm. Eng. 138 (2018) 583–590.

[15] F. Liu, K. Huang, L. Jiang, Promoted adsorption of CO_2 on amine-impregnated adsorbents by functionalized ionic liquids, AlChE J. 64 (2018) 3671–3680.

[16] M.B. Haider, Z. Hussain, R. Kumar, CO_2 absorption and kinetic study in ionic liquid amine blends, J. Mol. Liq. 224 (2016) 1025–1031.

[17] M. Pishnamazi, A.T. Nakhjiri, A.S. Taleghani, A. Marjani, A. Heydarinasab, S. Shirazian, Computational investigation on the effect of [Bmim][BF_4] ionic liquid addition to MEA alkanolamine absorbent for enhancing CO_2 mass transfer inside membranes, J. Mol. Liq. 314 (2020), 113635.

[18] N.A. Ramli, N.A. Hashim, M.K. Aroua, Supported ionic liquid membranes (SILMs) as a contactor for selective absorption of CO_2/O_2 by aqueous monoethanolamine (MEA), Sep. Purif. Technol. 230 (2020), 115849.

[19] F. Zhang, C. Fang, Y. Wu, Y. Wang, A. Li, Z. Zhang, Absorption of CO_2 in the aqueous solutions of functionalized ionic liquids and MDEA, Chem. Eng. J. 160 (2010) 691–697.

[20] L.M. Galán Sánchez, G.W. Meindersma, A.B. de Haan, Kinetics of absorption of CO_2 in amino-functionalized ionic liquids, Chem. Eng. J. 166 (2011) 1104–1115.

[21] J.G. Lu, C.T. Lu, Y. Chen, L. Gao, X. Zhao, H. Zhang, Z.W. Xu, CO_2 capture by membrane absorption coupling process: Application of ionic liquids, Appl. Energ. 115 (2014) 573–581.

[22] J.G. Lu, Z.Y. Lu, Y. Chen, J.T. Wang, L. Gao, X. Gao, Y.Q. Tang, D.G. Liu, CO_2 absorption into aqueous blends of ionic liquid and amine in a membrane contactor, Sep. Purif. Technol. 150 (2015) 278–285.

[23] H. Liao, H. Gao, B. Xu, Z. Liang, Mass transfer performance studies of aqueous blended DEEA-MEA solution using orthogonal array design in a packed column, Sep. Purif. Technol. 183 (2017) 117–126.

[24] D.F. Ma, C.Y. Zhu, T.G. Fu, X.G. Yuan, Y.G. Ma, An effective hybrid solvent of MEA/DEEA for CO_2 absorption and its mass transfer performance in microreactor, Sep. Purif. Technol. 242 (2020), 116795.

[25] W. Conway, S. Bruggink, Y. Beyad, W. Luo, I. Melián-Cabrera, G. Puxty, P. Feron, CO_2 absorption into aqueous amine blended solutions containing monoethanolamine (MEA), N, N-dimethylethanolamine (DMEA), N, N-diethylethanolamine (DEEA) and 2-amino-2-methyl-1-propanol (AMP) for post-combustion capture processes, Chem. Eng. Sci. 126 (2015) 446–454.

[26] W. Jiang, X. Luo, H. Gao, Z. Liang, B. Liu, P. Tontiwachwuthikul, X. Hu, A comparative kinetics study of CO_2 absorption into aqueous DEEA/MEA and DMEA/MEA blended solutions, AlChE J. 64 (2018) 1350–1358.

[27] B. Panigrahi, C.Y. Chen, Microfluidic retention of progressively motile zebrafish sperms, Lab Chip 19 (2019) 4033–4042.

[28] J. Li, H. An, A.P. Sasmito, A.S. Mujumdar, X. Ling, Performance evaluation of mass transport enhancement in novel dual-channel design of micro-reactors, Heat Mass Transfer. 56 (2020) 559–574.

[29] W. Li, F. Yang, X. Qu, C. Li, Wicking nanofence-activated boundary layer to enhance two-phase transport in microchannels, Langmuir 36 (2020) 15536–15542.

[30] Y. Liu, T. Zhang, L. Lv, Y. Chen, S. Tang, Mass transfer and droplet formation regime in a countercurrent mini-channel extractor, Chem. Eng. J. 402 (2020), 125383.

[31] B. Aghel, E. Heidaryan, S. Sahraie, S. Mir, Application of the microchannel reactor to carbon dioxide absorption, J. Clean. Prod. 231 (2019) 723–732.

[32] N. Akkarawatkhoosith, W. Nopcharoenkul, A. Kaewchada, A. Jaree, Mass transfer correlation and optimization of carbon dioxide capture in a microchannel contactor: A case of CO_2-rich gas, Energies 13 (2020) 5465.

[33] X. Luo, S. Liu, H. Gao, H. Liao, H. Zhang, Z. Liang, An improved fast screening method for blended amine-based solvents for post-combustion CO_2 capture, Energy Procedia 114 (2017) 1848–1854.

[34] Z. Zhou, B. Guo, B. Lv, H. Guo, G. Jing, Performance and reaction kinetics of CO_2 absorption into AMP solution with [Hmim][Gly] activator, Int. J. Greenh. Gas. Con 44 (2016) 115–123.

[35] S. Weisenberger, A. Schumpe, Estimation of Gas Solubilities in Salt Solutions at Temperatures from 273 K to 363 K, AlChE J. 42 (1996) 298–300.

[36] A.F. Portugal, P.W.J. Derks, G.F. Versteeg, F.D. Magalhães, A. Mendes, Characterization of potassium glycinate for carbon dioxide absorption purposes, Chem. Eng. Sci. 62 (2007) 6534–6547.

[37] Z. Zhou, G. Jing, L. Zhou, Characterization and absorption of carbon dioxide into aqueous solution of amino acid ionic liquid [N_{1111}][Gly] and 2-amino-2-methyl-1-propanol, Chem. Eng. J. 204–206 (2012) 235–243.

[38] A. Ahmady, M.A. Hashim, M.K. Aroua, Density, viscosity, physical solubility and diffusivity of CO_2 in aqueous MDEA+[bmim][BF_4] solutions from 303 to 333K, Chem. Eng. J. 172 (2011) 763–770.

[39] N. Di Miceli Raimondi, L. Prat, C. Gourdon, J. Tasselli, Experiments of mass transfer with liquid-liquid slug flow in square microchannels, Chem. Eng. Sci. 105 (2014) 169–178.

[40] W. Sun, Y. Liu, K. He, S. Wang, The phase distribution of gas-liquid two-phase flow in microimpacting T-junctions with different branch channel diameters, Chem. Eng. J. 333 (2018) 34–42.

[41] W.T. Zheng, K. Huang, Y.T. Wu, X.B. Hu, Protic ionic liquid as excellent shuttle of MDEA for fast capture of CO_2, AlChE J. 64 (2018) 209–219.

[42] S. Haase, D.Y. Murzin, T. Salmi, Review on hydrodynamics and mass transfer in minichannel wall reactors with gas-liquid Taylor flow, Chem. Eng. Res. Des. 113 (2016) 304–329.

[43] R.S. Abiev, C. Butler, E. Cid, B. Lalanne, A.M. Billet, Mass transfer characteristics and concentration field evolution for gas-liquid Taylor flow in milli channels, Chem. Eng. Sci. 207 (2019) 1331–1340.

[44] T.C. Thulasidas, M.A. Abraham, R.L. Cerro, Flow patterns in liquid slugs during bubble-train flow inside capillaries, Chem. Eng. Sci. 52 (1997) 2947–2962.

[45] M. Sattari-Najafabadi, M. Nasr Esfahany, Z. Wu, B. Sunden, Mass transfer between phases in microchannels: A review, Chem. Eng. Process. 127 (2018) 213–237.

[46] J. Yue, G. Chen, Q. Yuan, L. Luo, Y. Gonthier, Hydrodynamics and mass transfer characteristics in gas–liquid flow through a rectangular microchannel, Chem. Eng. Sci. 62 (2007) 2096–2108.

[47] C. Yao, Z. Dong, Y. Zhao, G. Chen, Gas-liquid flow and mass transfer in a microchannel under elevated pressures, Chem. Eng. Sci. 123 (2015) 137–145.

[48] M. Garcia, H.K. Knuutila, S. Gu, Determination of Kinetics of CO_2 Absorption in Unloaded and Loaded DEEA+MAPA Blend, Energy Procedia 114 (2017) 1772–1784.

[49] D.W. Van Krevelen, P.J. Hoftijzer, Kinetics of gas-liquid reactions part I. General theory, Recueil 67 (1948) 563–586.

[50] B. Lv, C. Sun, N. Liu, W. Li, S. Li, Mass transfer and kinetics of CO_2 absorption into aqueous monoethanolamine/1-hydroxyethy-3-methyl imidazolium glycinate solution, Chem. Eng. J. 280 (2015) 695–702.